Jordan Journal of Civil Engineering, Volume **16**, No. **3**, **2022**

Repair of Locally Corroded Reinforced Concrete Columns by FRP Sheets and Steel Jackets in Corrosive Environments

Mohamad Hossein Naserifard [1) *] ***and Mehdi Yazdian*** [2)]

[1)] Department of Civil Engineering, Yazd University, Yazd, Iran.
[2)] Faculty Member of Civil Engineering Department, Science & Arts University, Yazd, Iran.
* Corresponding Author. E-Mail: mh.naseri@stu.yazd.ac.ir

ABSTRACT

This paper aims to investigate the strengthening of locally corroded concrete columns using the combination of FRP sheets and steel jackets. In this regard, an analytical study is conducted using ABAQUS finite element program. The corroded zone has been strengthened using three methods including the use of FRP sheets, steel jackets and a combination of FRP sheets and steel jackets. It's worth mentioning that FRP sheets were mentioned in 1-layer and 2-layer cases and three different lengths, including 50% of the length of the corrosion zone, the entire length of the corrosion zone and the entire length of the corrosion zone in addition to 60% of the length of this zone in the upper part of the corrosion zone. By examining the results, it is concluded that strengthening corroded columns with 1-layer FRP sheets in the length of the corroded zone in addition to 60% of the corrosion zone length causes the greatest ductility. Furthermore, strengthening corroded concrete columns with steel jackets in combination with 2-layer FRP sheets in the length of the corroded zone in addition to 60% of the corrosion zone length causes the greatest strength and thus improves the structural behavior of the corroded columns.

KEYWORDS: FRP sheets, Steel jackets, Reinforced concrete columns, Corrosion, Corrosive environments.

INTRODUCTION

Many existing reinforced concrete columns may have insufficient strength and poor seismic performance due to the requirements of current codes. The retrofit of these columns can include coating the outer surface of the concrete to achieve the strength and deformability demands according to existing codes. So far, several experimental and analytical studies have investigated strengthening columns using fiber-reinforced polymer (FRP) (Rousakis and Karabinis, 2011). On the other hand, efficient maintenance of construction infrastructure, including highways, roads, railways, ports and airports, is critical and challenging. In addition, steel, wood and concrete structures are highly vulnerable to severe air attacks, such as chloride and sulfate penetration, especially in marine or mineral environments, which affects their integrity and impairs their performance (Mangi et al., 2019). Therefore, so far, steel jackets have been used to strengthen and retrofit reinforced concrete members with structural imperfections and to increase corrosion resistance (Abdel-Hay and Fawzy, 2015). Carbon fiber-reinforced polymer (CFRP) has also been used as a suitable alternative for seismic repairs and greater capacity (Wu and Pantelides, 2017). FRP composites are effective in restoring the strength of damaged wooden structures in marine piers, rehabilitation of steel bridges, strengthening of reinforced concrete bridges against severe corrosion and cracking, seismic repair of bridge columns with severe concrete crushing, … etc. to increase the strength and ductility of these structures (Hajsadeghi et al., 2011). Corrosive and acidic soils are other types of severe environments that cause significant structural damage and loss of performance of reinforced concrete structures (Bassuoni and Nehdi, 2009). Wu and

Received on 31/5/2021.
Accepted for Publication on 15/5/2022.

Pantelides (2018) incorporated the effect of bond-slip in the model they developed to accurately simulate the seismic performance of repaired column-to-cap beam/footing connections using CFR jacket. Del Zoppo et al. (2021) designed and tested four prefabricated reinforced concrete bridge columns with different levels of corrosion to investigate the seismic behavior under corrosion. The results show that the low corrosion level of longitudinal reinforcement (7.2%) has led to a significant reduction (15%) in lateral load capacity, energy dissipation and ductility. Therefore, retrofit of prefabricated reinforced concrete bridge columns should be carried out at a low corrosion level. Zhang et al. (2021) investigated rapid repair for earthquake-induced bending and shear damage at the bottom of reinforced concrete columns using a thin stainless-steel jacket around the column and external prestressed steel straps. The results showed that the ductility of the repaired samples was 111.4% higher than that of the original sample and the lateral force capacity was 113.3% higher than that of the original sample. Zhang et al. (2020) designed a prefabricated bridge column under cyclic loading. After performing a cyclic test on the designed column, carbon fiber-reinforced polymer (CFRP) sheets were used to repair damaged samples. The test results showed that the concrete damage of the repaired sample was reduced compared to that of the original sample and the repaired column had relatively more energy dissipation than the original column. Wang et al. (2021) suggested that high-strength reinforcement be used as a longitudinal reinforcement of reinforced concrete piers to reduce the permanent deformation of columns. In a study of Mahmoudabadi and Sakhaeipour (2020), analytical samples with square cross-sections and rectangular cross-sections have been studied. In each group, three samples without reinforcement, three samples with one layer and three samples with two layers of CFRP were considered. The results show that the cross-section of the column has no effect on the axial bearing capacity and the addition of CFRP layers has a great effect on the lateral bearing capacity of the column and unlike the axial bearing capacity, the presence of the second CFRP layer is very effective. By increasing the ratio of section length to width in rectangular specimens and by increasing the cross-sectional dimensions in square specimens, the effect of the number of CFRP layers on the axial and lateral bearing capacity and the energy absorbed by the column has decreased. In a study of Amoushahi and Ghasemitabar (2019), by placing glass fiber-reinforced polymer (GFRP) sheets on the beam flange, better results have been obtained than by the arrangement of GFRP sheets on the web.

Despite the approved efficiency of FRP, there is a lack of strengthening of existing corroded columns with the combination of FRP sheets and steel jackets. According to the aforementioned discussion and literature review, further research is needed to understand the behavior of corroded columns strengthened with the combination of FRP sheets and steel jackets. For this purpose, the current paper aims to generalize the combination of using FRP sheets and steel jackets in corroded columns. In this regard, firstly, the effect of corrosion on the cyclic behavior of the column was investigated considering different percentages of corrosion. Then, the corroded zone has been strengthened using three methods and the behaviors of these methods were compared to each other. Strengthening methods are: a) strengthening using FRP sheets, b) strengthening using steel jackets and c) strengthening using a combination of FRP sheets and steel jackets. It should be noted that finite element models are generated by ABAQUS and numerical results are compared with those of experimental tests conducted by Achillopoulou et al. (2012) and Alhawamdeh and Alqam (2020) to ensure modeling accuracy.

Development of the Finite Element Model

As mentioned before, finite element models are created by multi-purpose ABAQUS software. Both of the geometrical and material nonlinearities are considered for the performed general static analysis. It is worth mentioning that the column longitudinal reinforcements and stirrups are distributed at equal distances of 7.5 centimeters of the column height. Concrete parts of the finite element models were modeled using C3D8R element in ABAQUS. C3D8R is a higher-order 3-D 8-node solid element with reduced integration. Steel reinforcement parts of the models were modeled using a 2-node 3-D truss element called T3D2 element. A 4-node thin shell element with reduced integration called S4R element was used to model FRP sheets.

Material Behavior

The elastic concrete material behavior was defined by concrete Young's modulus (E_c) and concrete Poisson's ratio(ν_c) and the plastic behavior of concrete material was simulated with Concrete Damage Plasticity (CDP) by concrete compressive strength (f_c'), Poisson's ratio(ν_c), eccentricity(e), the ratio of the strength in the biaxial state to the strength in the uniaxial state (f_{b0}/f_{c0}), parameter K (ratio of the second stress invariant on the tensile meridian), viscosity parameter and dilation angle (ψ). It should be mentioned that the appropriate parameters for modeling of reinforced concrete members and concrete tensile and compressive strain-stress behavior were considered following the studies conducted by Rabi et al. (2019) and Rabi et al. (2021), respectively. Table 1 demonstrates the elastic and plastic properties of concrete.

Table 1. Elastic and plastic properties of concrete

Elastic properties of concrete							
ν_c				**E_c (MPa)**			
0.2				24667			
Plastic properties of concrete							
f_c' (MPa)	**f_t (MPa)**	**f_r (MPa)**	**Dilation angle (ψ)**	**Eccentricity (e)**	**f_{b0}/f_{c0}**	**K**	**Viscosity parameter**
27	3.1	3.5	36°	0.1	1.16	0.667	0

The material properties of longitudinal and transverse reinforcements and steel jackets used for all analytical models are shown in Table 2. These properties have been considered constant for all of the models which are modeled as bilinear elastoplastic materials in ABAQUS. In the proposed model, the longitudinal and transverse reinforcements and steel jackets behave as elastic materials before the applied stress reached the yield stress. Thereafter, the plastic deformation occurred continuously with a constantly increasing rate of stress up to the failure state. Like before, the elastic steel material behavior was defined by steel Young's modulus (E_s) and steel Poisson's ratio (ν_s). The yield stress of longitudinal reinforcements (F_{yl}), yield stress of transverse reinforcements (F_{yt}) and yield stress of the steel jacket (F_{yj}) are presented in Table 2.

Table 2. Steel material properties

E_s (MPa)	**ν_s**	**F_{yl} (MPa)**	**F_{yt} (MPa)**	**F_{yj} (MPa)**
200000	0.3	345	303	275

FRP sheets are modeled as a lamina linear elastic element using elastic modulus in the longitudinal direction (E_{11}), elastic modulus in the transverse direction (E_{22} and E_{33}), plane shear modulus (G_{12} and G_{13}), normal to plane shear modulus (G_{23}) and Poisson's ratio in plane direction (ν_{12}, ν_{13}) and normal to plane direction (ν_{23}), as shown in Table 3.

Table 3. Material properties of FRP sheets

E_{11}(GPa)	**$E_{22} = E_{33}$(GPa)**	**$G_{12} = G_{13}$(GPa)**	**G_{23}(GPa)**	**$\nu_{12} = \nu_{13} = \nu_{23}$**
41.5	3.82	1.45	1.53	0.33

Modeling of Interfaces

Different contact models can be used to simulate the interfacial behavior between two surfaces in ABAQUS. Since debonding between the concrete surface and FRP sheets does not occur during loading and the control failure mode is the rupture failure of FRP sheets (Lam et al., 2003; Ferrotto et al., 2018), in this paper, perfect bonding between the FRP sheets and the concrete was

assumed, which was achieved by tying FRP sheets to the concrete utilizing the tie option in ABAQUS (Lin and Teng, 2017; Panahi et al., 2021; Osama et al., 2021). The interaction between concrete and steel reinforcement is performed using an embedded constraint option that simulates a perfect bond action between the concrete and the steel bars (Lin and Teng, 2017; Osama et al., 2021).

Loading and Boundary Conditions

In the present study, a 0.1 $f_c'A_g$ axial load was applied centrally on the column top to simulate the axial dead load on the bridge piers. It should be noted that $f_c'$is the concrete compressive strength and A_g is the general cross-section of the concrete column. To assure a uniform distribution of the axially applied load, a rigid plate at the top of the column is used which can prevent the local failure of concrete due to stress concentration at the point of loading. The rigid plate is modeled using a 3D rigid element with four nodes (R3D4) and tied to the adjacent solid elements at the top of the column using the tie option. After the application of the axial load, the cyclic lateral displacement in terms of time (Figure 1(a)) is applied to the upper end of the column according to the schematic in Figure 1(b). The model is analyzed using a displacement control option and the axial load and lateral displacement are applied at the center point of the rigid plate, which is defined as the reference point of the rigid plate. The lower end of the column is restrained against displacements in all three directions in accordance with the actual end restraints and at the upper end of the column, all deformations are restrained at the reference point except translation in the z-direction.

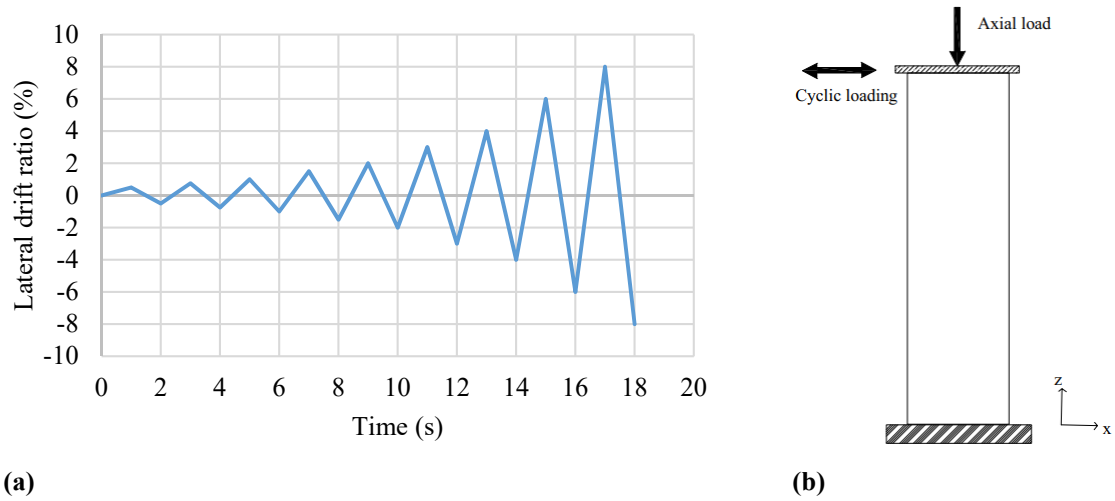

(a) **(b)**

Figure (1): a) Loading protocol and b) Boundary conditions

Verification of the Simulation

An experimental test by Achillopoulou et al. (2012) was utilized to calibrate the finite-element simulations of this study. As in the experimental test of Achillopoulou et al. (2012), the degrees of freedom at the upper end of the column, including motion and rotation, are restricted except for displacement along the vertical axis (Z) and the lower end of the column is considered fixed. Rectangular reinforced concrete column, with a length of 750 mm and a cross-section of 150×150 mm, was simulated to model the response of confined rectangular reinforced concrete columns with FRP sheets under axial loading. The mentioned column was reinforced longitudinally with 4 steel bars of 8 mm diameter (fy = 500 MPa) and laterally with steel ties of 5 mm diameter at a spacing of 100 mm except at the ends (25 mm spacing) and this is due to stress concentration at the ends. Also, these critical ends were additionally strengthened with two layers of FRP composite sheets for a distance of 125 mm. The plain concrete strength during the experiments was 13.4 MPa at a strain level of 2.2‰. As previously mentioned, C3D8R, T3D2 and S4R elements were used to simulate concrete parts, steel reinforcements and FRP sheets, respectively. The concrete column and FRP sheets modeled in ABAQUS are according to Figures 2(a) and 2(b), respectively. Figure 2(c) shows the meshing of column and FRP sheets in ABAQUS. To determine the appropriate mesh

density, a convergence study was carried out. Perfect bonding between concrete and FRP sheets was assumed using tie interaction in ABAQUS, which simulates the adhesion between concrete and FRP sheets. Figure 3 compares finite-element simulation results and the experimental results (Achillopoulou et al., 2012), which are in acceptable agreement.

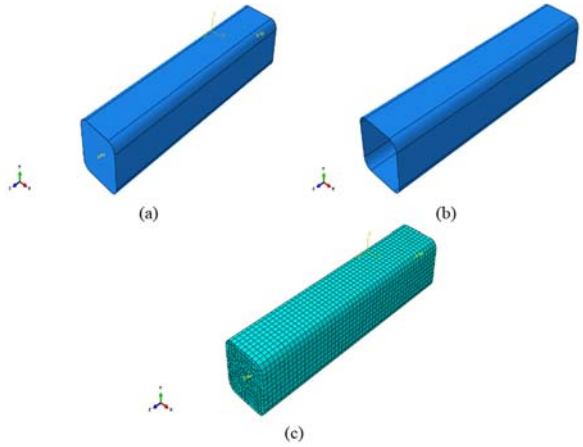

Figure (2): a) Concrete column modeled in ABAQUS, b) FRP modeled in ABAQUS and c) Finite element mesh of column and FRP sheets in ABAQUS

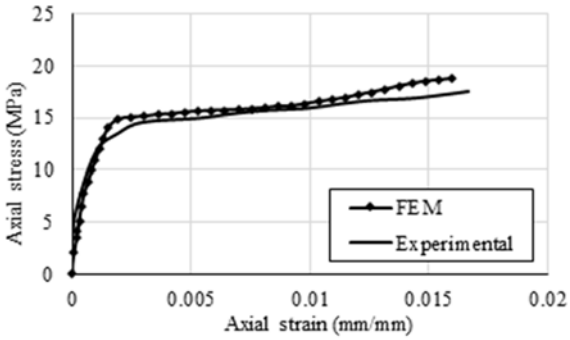

Figure (3): Comparison of FEM model and experimental results obtained by Achillopoulou et al. (2012)

Other verifications were carried out against experimental tests conducted by Alhawamdeh and Alqam (2020) to further validate the finite-element model. Alhawamdeh and Alqam (2020) tested twelve pin-ended concrete columns of 900 mm height and 150 × 150 mm cross-section subjected to axial loading. Four longitudinal reinforcements with a diameter of 12 mm are considered. In addition, transverse reinforcements with a diameter of 10 mm and a distance of 150 mm have been used. It should be noted that the compressive strength of concrete was 18 MPa and the yield stress of longitudinal and transverse reinforcements was 420 MPa and 280 MPa, respectively. In this paper, the experimental results of two of the specimens (specimen C1 without FRP sheets and specimen C7 with FRP sheets) are utilized to check the numerical results against the experimental ones. All of the models had an element size of approximately 10 mm based on a mesh convergence study. Perfect bonding between the FRP sheets and the concrete was assumed utilizing the tie option in ABAQUS. The steel bars were also assumed to be perfectly bonded to the adjacent concrete using the embedded option in ABAQUS. Axial loading was applied in the finite-element model through a rigid circular plate (rigid body) with zero thickness at the top surface of the column. Results achieved by numerical *versus* experimental outcome tested by Alhawamdeh and Alqam (2020) are depicted in Figure 4.

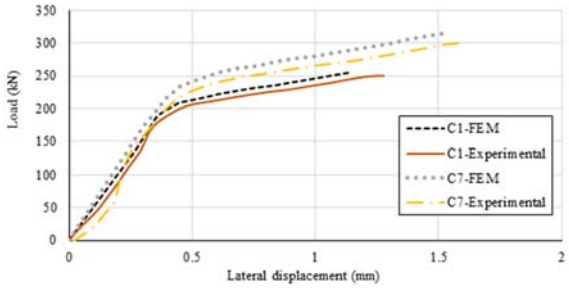

Figure (4): Comparison of load–deflection curves of FEM model and experimental results by Alhawamdeh and Alqam (2020)

The crack patterns obtained experimentally (Alhawamdeh and Alqam, 2020) and numerically for specimen C1 are depicted in Figure 5(a) and Figure 5(b), respectively. Tensile cracks in the columns in ABAQUS are outputted by the "PE Max Principle" option (legend for Figure 5(b)) and refer to the tensile plastic strain values in the concrete. As shown in Figure 5(a), the C1 specimen displayed brittle and compression failure and crack formation occurred on the compression side. Figures 6(a) and (b) show crack patterns obtained experimentally (Alhawamdeh and Alqam, 2020) and numerically for specimen C7. As shown in Figure 6(a), the C7 specimen failed in a relatively ductile manner due to the confinement of FRP wraps, which is in acceptable

agreement with numerical results, as shown in Figure 6(b).

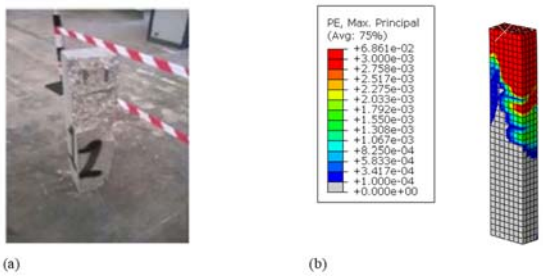

Figure (5): Failure modes for C1 specimen. a) Experimental (Alhawamdeh and Alqam, 2020) and b) Finite-element

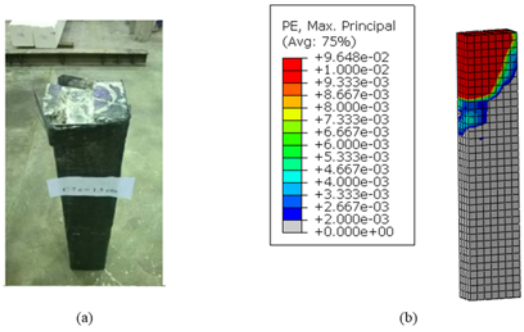

Figure (6): Failure modes for C7 specimen. a) Experimental (Alhawamdeh and Alqam, 2020) and b) finite-element

Based on the results, there is a reasonable correlation between the experimental model and the finite-element one. Thus, the finite-element model can predict the actual behavior of the concrete column confined with FRP sheets.

Simulating Corrosion Effect

As in a study conducted by Al-Salloum (2007), the reduced cross-sectional area of steel should be utilized to simulate the corrosion effect on steel reinforcements. According to the experimental work conducted by Al-Salloum (2007), by increasing the corrosion percentage, the ratio of the steel cross-sectional area to the initial steel cross-sectional area is reduced. The ratio of the steel cross-sectional area to the initial steel cross-sectional area for steel corrosion percentages of 8%, 19% and 33% is 0.85, 0.6 and 0.35, respectively. Accordingly, the steel cross-sectional area (longitudinal and transverse reinforcements) before and after corrosion was obtained as shown in Table 4. In the current study, in order to investigate the corrosion caused by cracking of the concrete, the cross-sectional area of each side of the concrete column was reduced by approximately 10 mm (equivalent to 8% corrosion), 25 mm (equivalent to 19% corrosion) and 40 mm (equivalent to 33% corrosion) (Al-Salloum, 2007).

Table 4. The cross-sectional area of longitudinal and transverse reinforcements before and after corrosion

Corrosion percentages	The ratio of the cross-sectional area after corrosion to the initial cross-sectional area	Initial longitudinal cross-sectional area	Initial transverse cross-sectional area	Longitudinal cross-sectional area after corrosion	Transverse cross-sectional area after corrosion
8	0.85	246.56	50.25	216.291	42.72
19	0.6	246.56	50.25	152.672	30.156
33	0.35	246.56	50.25	89	17.52

RESULTS AND DISCUSSION

The purpose of this study is to investigate the effect of using the combination of FRP sheets and steel jackets in corroded columns on the structural behavior of columns. In this section, a detailed study is carried out on the concrete columns for studying the effect of parameters, such as corrosion area length, corrosion percentage, column slenderness in the non-strengthened state and the effect of column strengthening using steel jackets and FRP sheets. For this purpose, the under-study concrete column is subjected to cyclic loading and finally, the push of the hysteresis curve was drawn and parameters, such as ductility, were extracted. It should be noted that the under-study column has cross-sectional dimensions of 500 × 500 mm and a height of 2500 mm.

The Effect of Corrosion on the Hysteresis Curves

In order to investigate the effect of corrosion on the hysteresis behavior of concrete columns, a concrete column with a corroded length of 500 mm from the end has been modeled in ABAQUS finite element software. The schematic shape of the locally corroded column (part B) is given in Figure 7 .This study was evaluated for different corrosion percentages including 8%, 19% and 33%, as shown in Table 5. The cyclic curve of the columns under different corrosions is given in Figure 8. According to Figure 8, it is obvious that by increasing the percentage of corrosion, the strength of the models in different cycles has decreased compared to the base model without corrosion. In addition, by increasing the corrosion percentage, the slope of the downward resistance zone has slightly increased, which can be attributed to the increase in cracking due to more corrosion. Furthermore, it is obvious that in the last cycles, the strength reduction occurs faster.

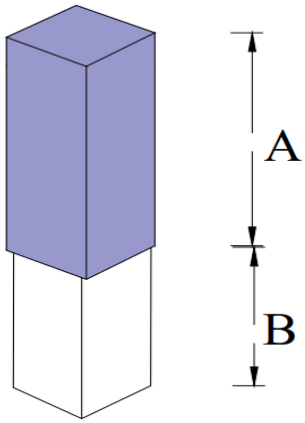

Figure (7): The schematic figure of locally corroded column (part B)

Table 5. Specifications of the models to investigate the effect of corrosion percentage

Model	Length of the corroded zone (mm)	Corrosion percentage	Column slenderness coefficient
M500- 34(Base model)	-	-	34
M500-C8%-34	500	8	34
M500-C19%-34	500	19	34
M500-C33%-34	500	33	34

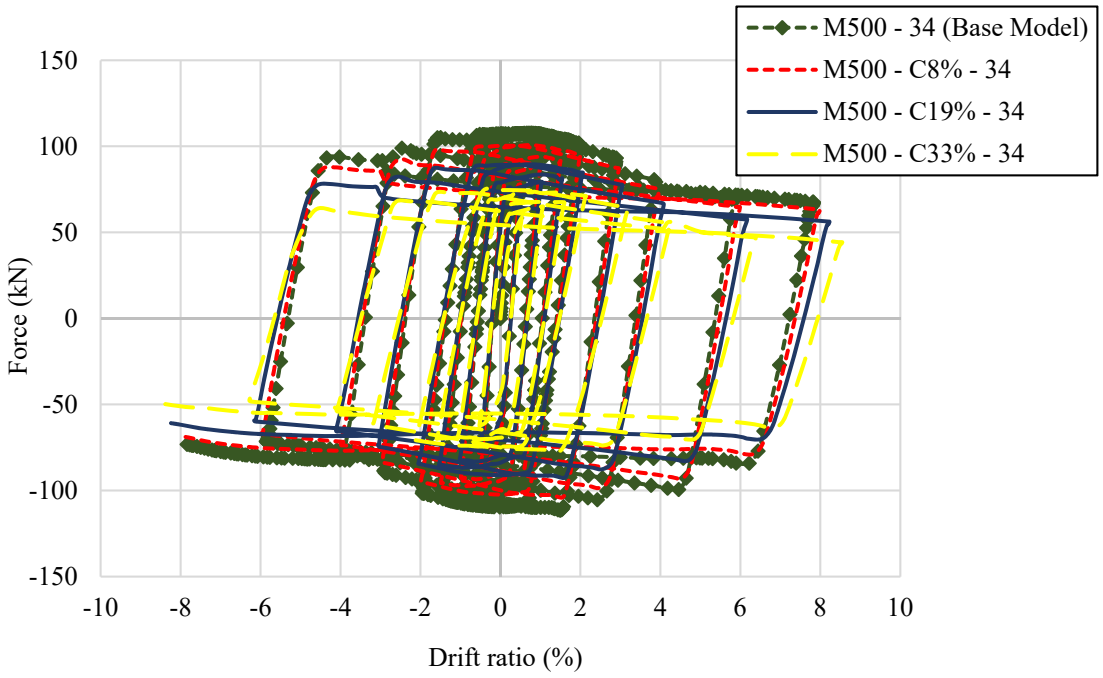

Figure (8): Effect of corrosion on cyclic curves

The cracking processes of corroded concrete columns at different loading moments are shown in Figures from 9 to 11. According to the mentioned figures, it is clear that cracks have started to spread from the end of the column and the area of corrosion (Figure 9). Gradually, in the last cycles of the loading protocol, the entire corrosion area cracks (Figure 10). It is obvious that at the end of loading, the cracks have spread to the top of the corroded zone (Figure 11). It can be noticed that by decreasing the strength of the models due to increasing the percentage of corrosion, brittle failure of the specimens occurs earlier compared to the base model without corrosion.

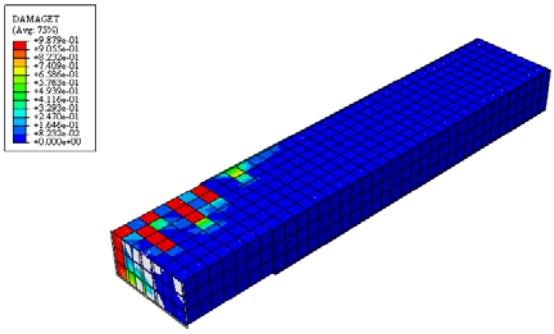

Figure (9): Cracks start to appear in the corrosion zone of the concrete column at 12.5 mm displacement

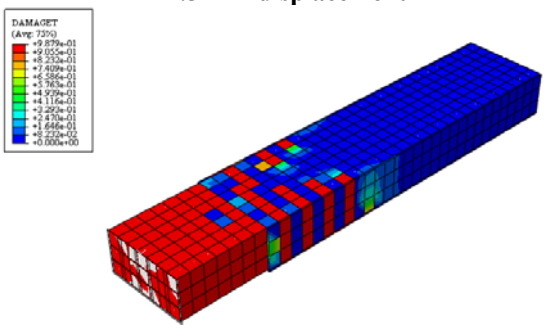

Figure (10): The ongoing process of cracking for the concrete column in the corrosion zone at 50 mm displacement

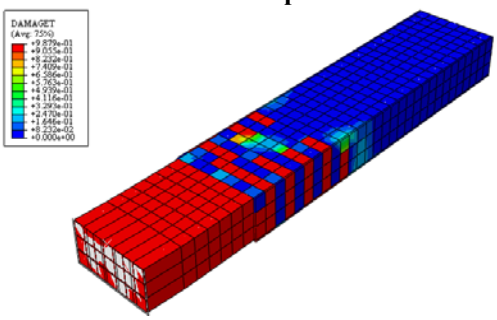

Figure (11): The ongoing process of cracking for the concrete column in the corrosion zone at 200 mm displacement

The Effect of Column Slenderness on the Hysteresis Curves

To investigate the slenderness effect, concrete columns with different slenderness coefficients according to Table 6 have been subjected to cyclic loading. The slenderness of the columns was considered 20 (equivalent to the length of 1500 mm), 34 (equivalent to the length of 2500 mm) and 50 (equivalent to the length of 3500 mm). It should be mentioned that in order to investigate the effect of slenderness, models with 33% corrosion percentage along 1000 mm of the column end and identical cross-sectional area were used. According to Figure 12, which shows the push of hysteresis curves of the concrete columns with different slenderness values, it is clear that increasing the slenderness has reduced the maximum strength. It should be noted that this reduction for the two slenderness values of 34 and 50 was much greater than the reduction for the slenderness value of 20. Furthermore, by increasing the slenderness value from 34 to 50, the maximum strength has reduced about 69% and by increasing the slenderness value from 20 to 34, the maximum strength has reduced about 57%. Moreover, according to Figure 12, it is clear that by decreasing the slenderness value the strength deterioration occurs faster.

Table 6. Specifications of the models to evaluate the effect of column slenderness

Model	Length of the corroded zone (mm)	Corrosion percentage	Column slenderness value
M1000-C33%-20	1000	33	20
M1000-C33%-34	1000	33	34
M1000-C33%-50	1000	33	50

Methods of Strengthening Concrete Columns

The purpose of this paper is to investigate the effect of corrosion on the structural behavior of the column and then the strengthening of the corroded column by FRP sheets, steel jackets and a combination of FRP sheets and steel jackets. In this regard, the effect of different methods of strengthening locally corroded concrete columns has been investigated (as shown in Table 7). The base model, in this case, is a reinforced concrete

column with a slenderness of 34, where the concrete compressive strength is 40 MPa, the axial load is 0.1 $f_c'A_g$, the corrosion zone length is 750 mm and the corrosion percentage is 19%.

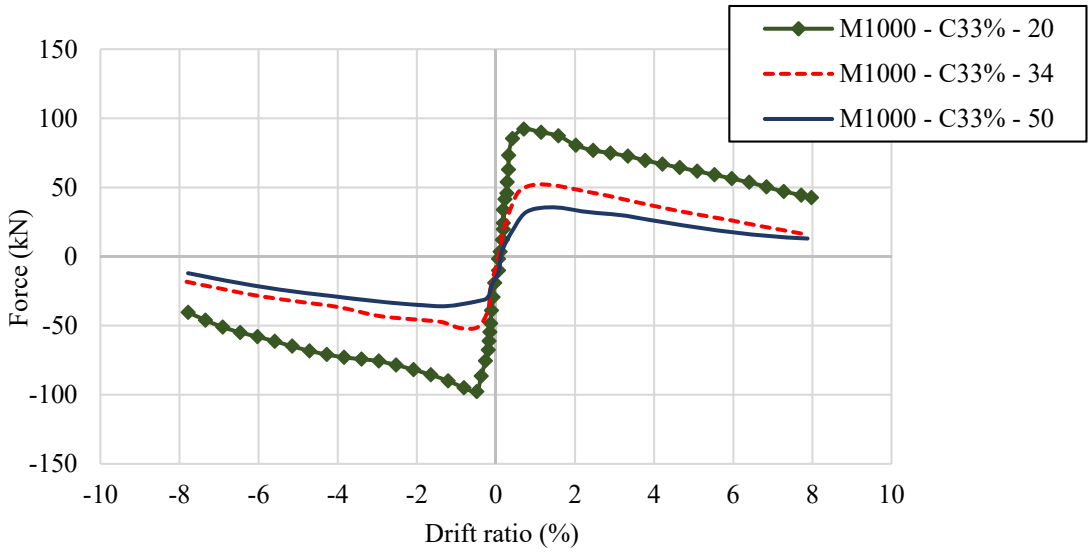

Figure (12): Push of hysteresis curves of the models with different slenderness values

Table 7. Specifications of the models to evaluate the column strengthening methods

Model	Strengthening method	Length of the strengthened area with FRP sheets (mm)	Length of the strengthened area with steel jacket (mm)	Number of FRP layers
M750-C19% (Base model)	-	-	-	-
FRP375-1Layer	FRP sheets	375	-	1
FRP375-2Layers	FRP sheets	375	-	2
FRP750-1Layer	FRP sheets	750	-	1
FRP750-2Layers	FRP sheets	750	-	2
FRP1200-1Layer	FRP sheets	1200	-	1
FRP1200-2Layers	FRP sheets	1200	-	2
SJ750	steel jacket	-	750	-
SJ750-FRP750-1Layer	combination of steel jacket and FRP sheets	750	750	1
SJ750-FRP750-2Layers	combination of steel jacket and FRP sheets	750	750	2
SJ750-FRP1200-1Layer	combination of steel jacket and FRP sheets	1200	750	1
SJ750-FRP1200-2Layers	combination of steel jacket and FRP sheets	1200	750	2

The first strengthening method was using FRP sheets around the column. According to Table 7, the base model was strengthened using 1-layer and 2-layer FRP sheets in a length of 375, 750 and 1200 mm. Due to the length of the corrosion zone (750 mm), it's worth mentioning that FRP sheets in a length of 375 mm correspond to 50% of the length of the corrosion zone and FRP sheets in a length of 1200 mm correspond to

the entire corrosion zone in addition to 60% of the length of this zone in the upper part of the corrosion zone. The second strengthening method was using a steel jacket around the column. In this case, the base model was strengthened using a steel jacket with a length of 750mm. Finally, in the third strengthening method (combination of FRP sheets and steel jackets), first, the column was strengthened with a steel jacket and then, FRP sheets were added. In this method, the base model was strengthened using a steel jacket with a length of 750 mm and FRP sheets with a length of 750 and 1200 mm, which were considered in 1-layer and 2-layer cases. Figure 13 demonstrates the schematic figures of the strengthening methods. It is worthy to note that strengthening of the different lengths of the upper part of the corrosion zone can be considered as a parametric study in future studies.

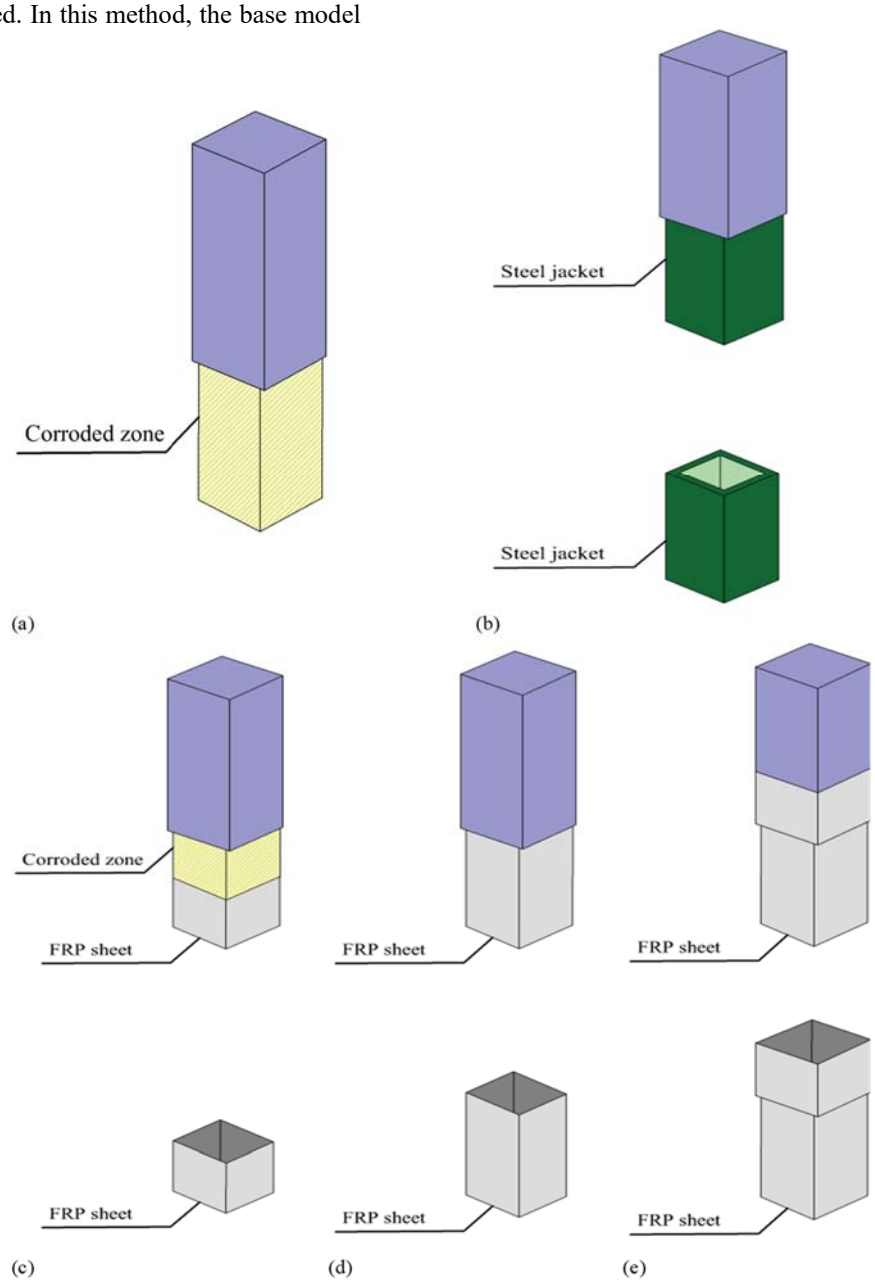

Figure (13): a) The schematic figure of the locally corroded column, b) Column strengthened with a steel jacket, c) Column strengthened with FRP sheet in a length of 375 mm, d) Column strengthened with FRP sheet in a length of 750 mm and e) Column strengthened with FRP sheet in

The force-drift ratio curves were depicted for all of the models according to Figure 14. Parameters, such as P_y (yield strength), P_{max} (maximum strength), P_u (ultimate strength), δ_y (displacements related to yield

strength), δ_{max} (displacements related to maximum strength), δ_u (displacements related to ultimate strength) and μ (ductility), were extracted and finally, their behaviors were compared with each other. It should be noted that parameter μ is the ductility of the models, which is obtained by dividing δ_u by δ_y. The results of the mentioned parameters are given in Table 8.

As shown in Figure 14, according to the FRP375-1Layer model, strengthening of the concrete column using 1-layer FRP sheets with a length of 375 mm has increased the maximum strength (3.4%) and ductility (5%) compared to the unstrengthened case (base model). On the other hand, in the FRP375-2Layers model, the maximum strength (4%) and ductility (23%) have increased compared to the unstrengthened case. In the case of FRP750-1Layer, the maximum strength will increase by 28% and ductility will become about twice compared to the unstrengthened case. The maximum strength in the FRP750-2Layers model will increase by 44.5% and ductility will become about twice compared to the unstrengthened case. Also, with increasing the length of the strengthened area from 375 to 750mm, the amount of ductility was approximately increased 53% in 2-layer FRP sheets and this increase was 81% in 1-layer FRP sheets. According to the FRP1200-1Layer model, the maximum strength has increased by 31% and ductility was 2.04 times that of the unstrengthened concrete column. On the other hand, using 1200 mm 2-layer FRP sheets, the maximum strength has increased by 58% and ductility was 1.96 times that of the unstrengthened concrete column. With a little care in Table 8, it is clear that in the case of 1200 mm FRP, compared to the case of 750 mm FRP, the strength has increased by 2.5% and the ductility has increased by approximately 7%. It should be noted that the use of 2-layer FRP sheets along the corroded zone length has a greater effect than the use of 1200-mm FRP coverage. So, the maximum strength has increased by 9.5%.

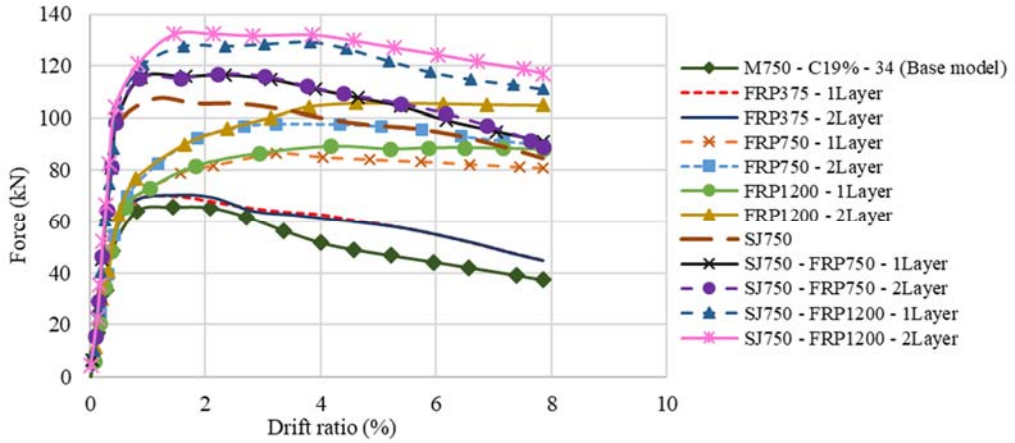

Figure (14): Force-drift ratio curves of different strengthening models

Table 8. The results obtained from the force-drift ratio curves

Specimen	P_y(N)	δ_y(mm)	P_{max}(N)	δ_{max}(mm)	P_u(N)	δ_u(mm)	μ
M750-C19% -34 (BASE MODEL)	61650.4	4.08	68446.6	24.30	58737.8	73.25	17.93
FRP375-1Layer	51757.3	5.89	70826.0	40.17	60198.3	111.04	18.85
FRP375-2 Layers	51199.4	5.44	71169.3	44.58	60488.0	120.54	22.16
FRP750-1 Layer	50843.1	5.85	88053.8	93.47	74845.7	200	34.19
FRP750-2 Layers	53208.4	5.86	98954.1	85.17	84110.9	200	34.10
FRP1200-1 Layer	50873.6	5.45	90335.9	163.59	76785.5	200	36.71
FRP1200-2 Layerss	54307.4	5.70	108011	116.31	91809.3	200	35.09
SJ750	74141.0	5.75	108084	24.67	90887.4	188.41	32.77
SJ750-FRP750-1 Layer	78606.4	5.86	118842	21.57	101088	148.38	25.32
SJ750-FRP750-2 Layer	69608.8	4.70	119459	26.67	101526	154.72	32.92
SJ750-FRP1200-1 Layer	86647.4	6.97	130828	62.72	111187	187.21	26.84
SJ750-FRP1200-2 Layers	80411.9	5.86	133765	40.08	113687	166.23	28.34

According to SJ750-FRP750-1Layer model, the maximum strength has increased compared to all previous conditions. Compared to the column without strengthening, the maximum strength was increased about 73%, while ductility, in this case, is less than the case of FRP750-1Layer. This could be justified in the way that in the initial cycles due to the presence of steel jacket in combination with FRP sheets, the strength has increased more than in the previous cases and in the following cycles, due to the yield of steel jacket materials, the strength will decrease with a greater slope, which will result in a lower ductility. In the case of SJ750 model and SJ750-FRP750-2Layers model, almost the same ductility has been obtained. The difference is that the strength in the case of SJ750-FRP750-2Layers model has increased by 11% compared to the case of SJ750 model. Also, in the SJ750-FRP1200-1Layer and SJ750-FRP1200-2Layers models, the highest strength and the least ductility have been obtained compared to all previous cases. In this case, the maximum strength has increased by 95% compared to the unstrengthened column.

Therefore, according to all the above and according to Table 8, it can be understood that in all of these models, the highest ductility is related to the cases where FRP coverage has been used alone. Meanwhile, concrete columns with 1-layer FRP coverage along the entire length of the corrosion zone and the upper 60% of it, have the highest ductility. Furthermore, the highest strength is related to the cases in which steel jackets have been used and among these, strengthening with steel jacket in combination with 2-layer FRP sheets along the entire length of the corrosion zone and the upper 60% of it has provided the highest strength.

It can be noticed that the maximum strength and elastic stiffness of the specimens increased in the case of using FRP sheets and steel jackets. It should be noted that the unstrengthened specimens displayed brittle failure at low force values, but strengthened specimens using steel jackets and FRP sheets displayed ductile failure due to the confinement of FRP sheets and steel jackets, especially in the case of using steel jacket in combination with 1-layer and 2-layer FRP sheets.

CONCLUSIONS

The purpose of this study is to investigate the effect of using the combination of FRP sheets and steel jackets in corroded columns on the structural behavior of columns. For this purpose, a detailed study is carried out on concrete columns for studying the effect of parameters, such as corrosion area length, corrosion percentage, column slenderness in the non-strengthened state and the effect of column strengthening using steel jackets and FRP sheets. Regarding the obtained results of this research, the most highlighted conclusions are as follows:

1. The results showed that by increasing the percentage of corrosion, the strength of the models in different cycles has decreased compared to the base model without corrosion. In addition, by increasing the corrosion percentage, the slope of the downward resistance zone has slightly increased, which can be due to the increase in cracking due to more corrosion. Furthermore, it is obvious that in the last cycles, the strength reduction occurs faster.
2. By increasing the slenderness from 34 to 50, the maximum strength has reduced about 69% and by increasing the slenderness from 20 to 34, the maximum strength has reduced about 57%.
3. By increasing the length of the strengthened area from 375 to 750mm, the amount of ductility was approximately increased 53% in 2-layer FRP sheets and this increase was 81% in 1-layer FRP sheets.
4. The highest ductility is related to the cases where FRP coverage has been used alone. Meanwhile, concrete columns with 1-layer FRP coverage along the entire length of the corrosion zone and the upper 60% of it (the length of 1200 mm), has the highest ductility.
5. The highest strength is related to the cases in which steel jackets have been used and among these, strengthening with steel jacket in combination with 2-layer FRP sheets along the entire length of the corrosion zone and the upper 60% of it (the length of 1200 mm) has provided the highest strength.

REFERENCES

ABAQUS/CAE User's Manual. Version 2016. SIMULIA.

Abdel-Hay, A.S., and Fawzy, Y.A.G. (2015). "Behavior of partially defected R.C columns strengthened using steel jackets". HBRC Journal, 11 (2), 194-200.

Achillopoulou, D.V., Rousakis, T.C., and Karabinis, A. (2012). "Square reinforced concrete columns strengthened through fiber-reinforced polymer (FRP) sheet straps". Proceedings of the 2012 6th International Conference on FRP Composites in Civil Engineering, June 13th-15th, Rome.

Alhawamdeh, M., and Alqam, M. (2020). "Behaviour assessment of reinforced concrete columns externally rehabilitated with carbon fiber-reinforced polymers (CFRPs) subjected to eccentric loadings". Jordan Journal of Civil Engineering, 14 (1).

Al-Salloum, Y.A. (2007). "Influence of edge sharpness on the strength of square concrete columns confined with FRP composite laminates". Composites, Part B, 38 (5-6), 640-650.

Amoushahi, H., and Ghasemitabar, M. (2019). "Static analysis of steel plates and sections retrofitted with FRP plates by finite-element modeling". Journal of Structural and Construction Engineering, 6 (3), 107-131.

Bassuoni M.T., and Nehdi, M.L. (2009). "Durability of self-consolidating concrete to sulfate attack under combined cyclic environments and flexural loading". Cement and Concrete Research, 39 (3), 206–226.

Del Zoppo, M., Menna, C., Di Ludovico, M., Asprone, D., and Prota, A. (2021). "Experimental evaluation of seismic performance of corroded precast RC bridge columns and the retrofit measure using CFRP jackets". Engineering Structures, 245, 112872.

Ferrotto, M.F., Fischer, O., and Cavaleri, L. (2018). "A strategy for the finite element modeling of FRP-confined concrete columns subjected to preload". Eng. Struct., 173, 1054-1067. https://doi.org/10.1016/j.engstruct.2018.07.047.

Ferrotto, M.F., Fischer, O., and Niedermeier, R. (2018). "Experimental investigation on the compressive behavior of short-term preloaded carbon fiber-reinforced polymer-confined concrete columns". Structural Concrete., 19 (4), 988-1001. https://doi.org/10.1002/suco.201700072.

Hajsadeghi, M., Alaee, F.J., and Shahmohammadi, A. (2011). "Investigation on behaviour of square/rectangular reinforced concrete columns retrofitted with FRP jacket". Journal of Civil Engineering and Management, 17 (3), 400-408.

Ho, N.M., Lima, M.M., and Doh, J.H. (2016). "Axially loaded three-side restrained reinforced concrete walls: A comparative study". Proceedings of the 24th Australian Conference on the Mechanics of Structures and Materials (ACMSM24), December 6th-9th, Perth, Australia.

Lam, L., and Teng, J.G. (2003). "Design-oriented stress-strain model for FRP-confined concrete in rectangular columns". Journal of Reinforced Plastics and Composites, 22 (13), 1149-1186.

Lin, G., and Teng, J. (2017). "Three-dimensional finite-element analysis of FRP-confined circular concrete columns under eccentric loading". Journal of Composites for Construction., 21(4), 4017003.

Mahmoudabadi, M., and Sakhaeipour, F. (2020). "Numerical analysis on the influence of the cross-section of ultimate capacity of reinforced concrete columns reinforced with CFRP". Journal of Structural and Construction Engineering, 7, 2476-3977.

Mangi, S.A., Wan Ibrahim, M.H., Jamaluddin, N., Arshad, M.F., and Shahidan, S. (2019). "Performances of concrete containing coal bottom ash with different fineness as a supplementary cementitious material exposed to seawater". Engineering Science and Technology: An International Journal, 22 (3), 929-938.

Osama, A., Aya, A., Eehab, K., and Hany, M. (2021). "Numerical investigation of FRP-confined short square RC columns". Construction and Building Materials, 275, 122141.

Panahi, M., Zareei, S.A., and Izadi, A. (2021). "Flexural strengthening of reinforced concrete beams through externally bonded FRP sheets and near-surface mounted FRP bars". Case Studies in Construction Materials, 15, e00601.

Rabi, M., Cashell, K.A., and Shamass, R. (2021). "Ultimate behaviour and serviceability analysis of stainless steel-reinforced concrete beams". Engineering Structures, 248, 113259.

Rabi, M., Cashell, K.A., and Shamass, R.J.E.S. (2019). "Flexural analysis and design of stainless steel-reinforced concrete beams". Engineering Structures, 198, 109432.

Rousakis, T.C. (2005). “Mechanical behaviour of concrete confined by composite materials”. Ph.D. Thesis, Civil Engineering Dept., Democritus Univ. of Thrace, Xanthi, Greece.

Rousakis, T.C., and Karabinis, A.I. (2012). “Adequately FRP confined reinforced concrete columns under axial compressive monotonic or cyclic loading”. Materials and Structures, 45 (7), 957-975.

Wang, J.H., Sun, Y.P., and Takeuch, T. (2021). “Seismic fragility and post-earthquake reparability of circular reinforced concrete bridge columns with low-bond high-strength reinforcements”. Structures, 34, 840-855.

Wu, R.Y., and Pantelides, C.P. (2017). “Rapid seismic repair of reinforced concrete bridge columns”. ACI Structural Journal, 114 (5), 1339.

Wu, R.-Y., and Pantelides, C.P. (2018). “Concentrated and distributed plasticity models for seismic repair of damaged RC bridge columns”. Journal of Composites for Construction, 22 (5), 04018044.

Zhang, D., Li N., Li, Z.X., and Xie, L. (2021). “Rapid repair of RC bridge columns with prestressed stainless-steel hoops and stainless-steel jackets”. Journal of Constructional Steel Research, 177, 106441.

Zhang, Y., Tabandeh, A., and Gardoni, P. (2020). “Seismic performance of precast segmental bridge columns repaired with CFRP wraps”. Composite Structures, 23, 112218.